



**FACULTY OF
PHYSICS**
UNIVERSITY
OF WARSAW

Primordial black holes, dark matter and gravitational waves with light scalars

Zygmunt Lalak
University of Warsaw

with **P. Michalak, A. Ghoshal, O. Ozsoy, M. Lewicki, P. Olszewski,
T. Krajewski**

arXiv:1402.3826 (JHEP), arXiv: 2103.03225, arXiv:1605.06713 (PRD),
arXiv:1411.6435 (PRD), arXiv:1606.07808 (JHEP), arXiv:1508.03297 (JHEP)
arXiv:1608.05719 (JCAP), arXiv:1711.08473 (JHEP) **Phys. Rev. D 104, 123522, JCAP
01 (2021) 040, JCAP (2023), JCAP 07 (2007) 014**

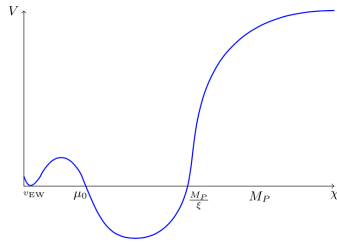
Corfu Summer Institute, September 3rd 2023

Outline:

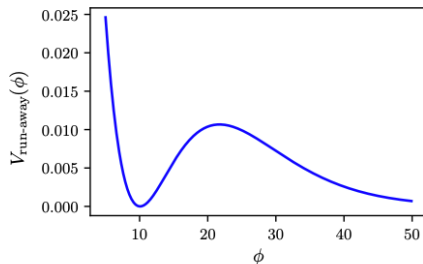
- SM and BSM effective potentials with non-equivalent vacua
- Domain walls and gravitational waves
- Bumpy axion inflation
- Non-minimal curvaton revisited
- Summary

Models of interest

- Radiatively generated minima (eg SM at large field strength)



- Run-away potentials (moduli of stringy models), Quantum Scale Symmetric SM



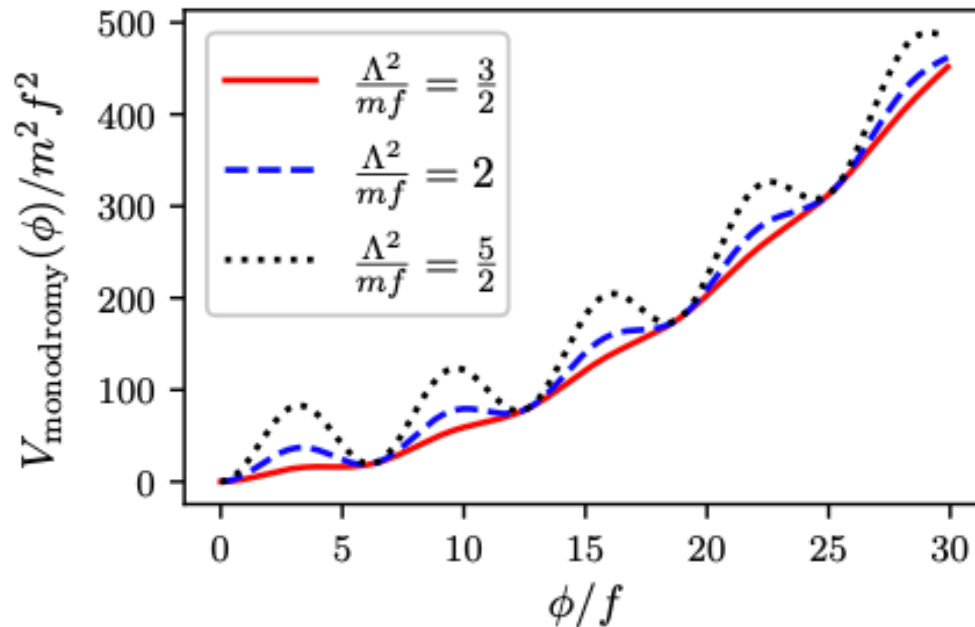
- Models of strong first-order phase transitions - colliding bubbles (thermal effects play a role)

Models of interest

- Monodromy axion models, relaxion

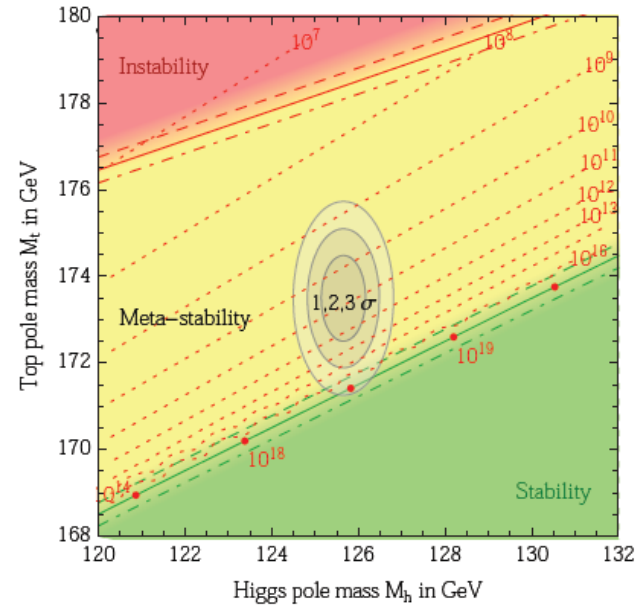
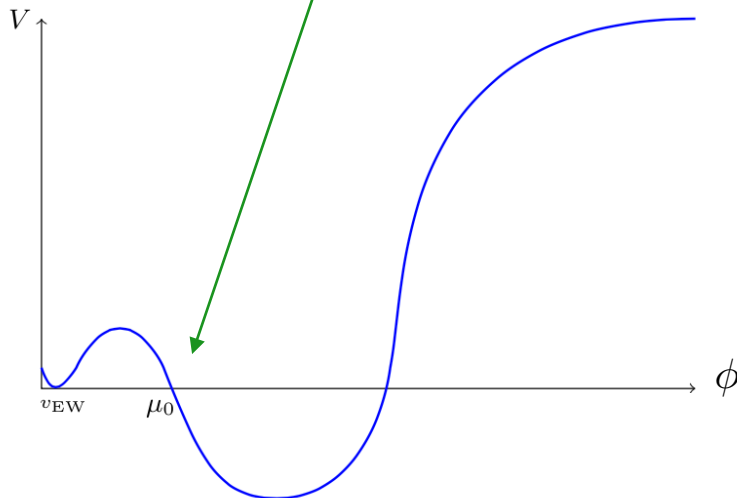
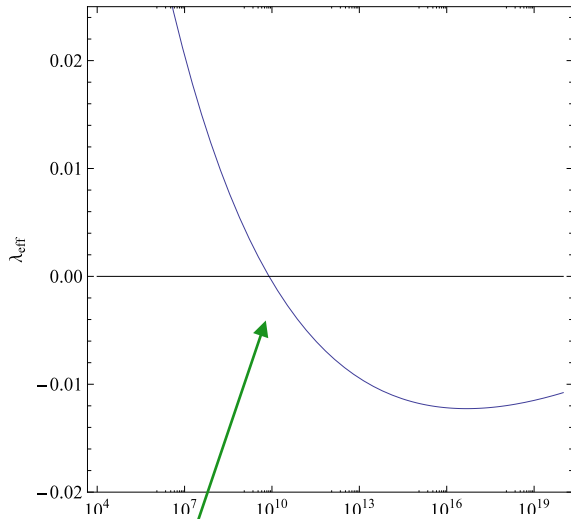
$$V_{\text{monodromy}}(\phi) = m^2 \phi^2 + \Lambda^4 \left[1 - \cos \left(\frac{\phi}{f} \right) \right]$$

$$V_{\text{relaxion}}(\phi) = g\phi + \Lambda^4 \left[1 - \cos \left(\frac{\phi}{f} \right) \right]$$



SM Metastability

$$\lambda_{\text{eff}} < 0 \implies \text{Metastability}$$



D. Buttazzo, et al. [arXiv:1307.3536].

G. Degrassi, et al. [arXiv:1205.6497].

See lectures by G. Degrassi Corfu 2014

SM + dilaton

with D. Ghilencea, P. Olszewski, P. Michalak

Quantum scale symmetric effective lagrangian

No scale anomaly in

$$\mathcal{L}^{(0)}(\phi, \sigma) = \frac{1}{2}(\partial\phi)^2 + \frac{1}{2}(\partial\sigma)^2 - \underbrace{\mu^{2\varepsilon}(\sigma)}_{\text{„dynamical” regulator}} \left[\underbrace{V(\phi, \sigma)}_{\text{renormalizable, classically scale-invariant}} + \sum_{n=0} \lambda_n \frac{\phi^{4+2n}}{\sigma^{2n}} \right]$$

$$\mathbb{Z}^2 \times \mathbb{Z}^2$$

$$\phi \rightarrow -\phi$$

$$\sigma \rightarrow -\sigma$$

go to broken phase

$$\mathcal{L}^{(0)}(\phi_0 + \phi', \sigma_0 + \phi')$$

compute loop corrections (in momentum expansion) & RGE functions β, γ

$$\mathcal{L}_{\text{eff}}(\phi, \sigma) = -V_{\text{eff}}(\phi, \sigma) + \dots$$

- Homogenous function (no mass-parameters, only vev's)
- $\mathbb{Z}^2 \times \mathbb{Z}^2$ sym.
- Satisfies Callan-Symanzik eq.

Quantum scale symmetric effective lagrangian

RG-improvement:

$$\mu = e^t \mu_0, \quad \lambda(t) \phi^4 + \frac{\lambda^2(t) \phi^4}{64\pi^2} \log \left(\frac{\phi}{e^t \sigma} \right)^2 + \dots \quad \leftarrow \quad \text{Choose } t = t(\phi, \sigma) \sim \log \frac{\phi}{\sigma} \text{ to avoid large logs.}$$

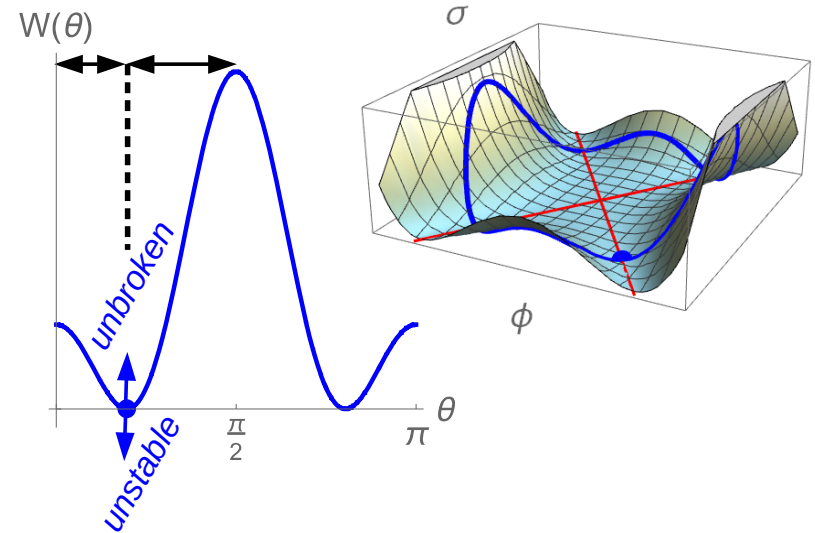
Spontaneous scale-symmetry breaking:

$$\begin{pmatrix} \phi \\ \sigma \end{pmatrix} = M \begin{pmatrix} \sin \theta \\ \cos \theta \end{pmatrix}, \quad V_{\text{eff}} = M^4 W(\theta),$$

flat direction in $V_{\text{eff}} \Rightarrow$

$$\exists_{\theta=\theta_0} W(\theta_0) = W'(\theta_0) = 0$$

*renormalization condition,
similar to choosing C.C.*



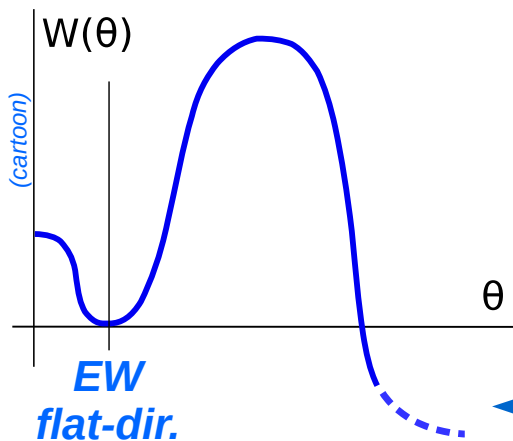
- **Hierarchy** of scales via **aligning** the flat direction $\perp \phi \rightarrow \theta_0 \approx \frac{\phi_0}{\sigma_0} \ll 1$
- New perspective on **naturalness**: is this alignment stable wrt. embedding in a UV completion?

Quantum scale symmetric SM + σ

$$H = \begin{pmatrix} 0 \\ \frac{\phi}{\sqrt{2}} \end{pmatrix} \quad (\text{electroweak vacuum} \longrightarrow \text{electroweak flat direction})$$

$$\mathcal{L}_{SM} \Big|_{\substack{m^2=0 \\ \mu = \mu(\sigma)}} + \frac{1}{2} (\partial\sigma)^2 - \lambda_m |H|^2 \sigma^2 - \frac{\lambda_\sigma}{4} \sigma^4 + \sum_{n=0} \lambda_n \frac{|H|^{4+2n}}{\sigma^{2n}}$$

$$V_{\text{eff}}^{\text{SM}}(\phi, \sigma) \approx \frac{1}{4} \lambda_{\text{eff}} \left(\log \frac{\phi}{\sigma} \right) \phi^4 = M^4 \underbrace{\lambda_{\text{eff}}(\log \tan \theta)}_{W(\theta)} \frac{\tan^4 \theta}{(1 + \tan^2 \theta)^2}$$



V_{eff} is:

- *unstable*
- *unbounded below*

Tunneling via **2-dim instanton** (Coleman's bounce), in the presence of nonrem. terms.

(Even stronger) motivation to stabilise the V_{eff} completely: $\lambda_{\text{eff}} \stackrel{!}{>} 0$

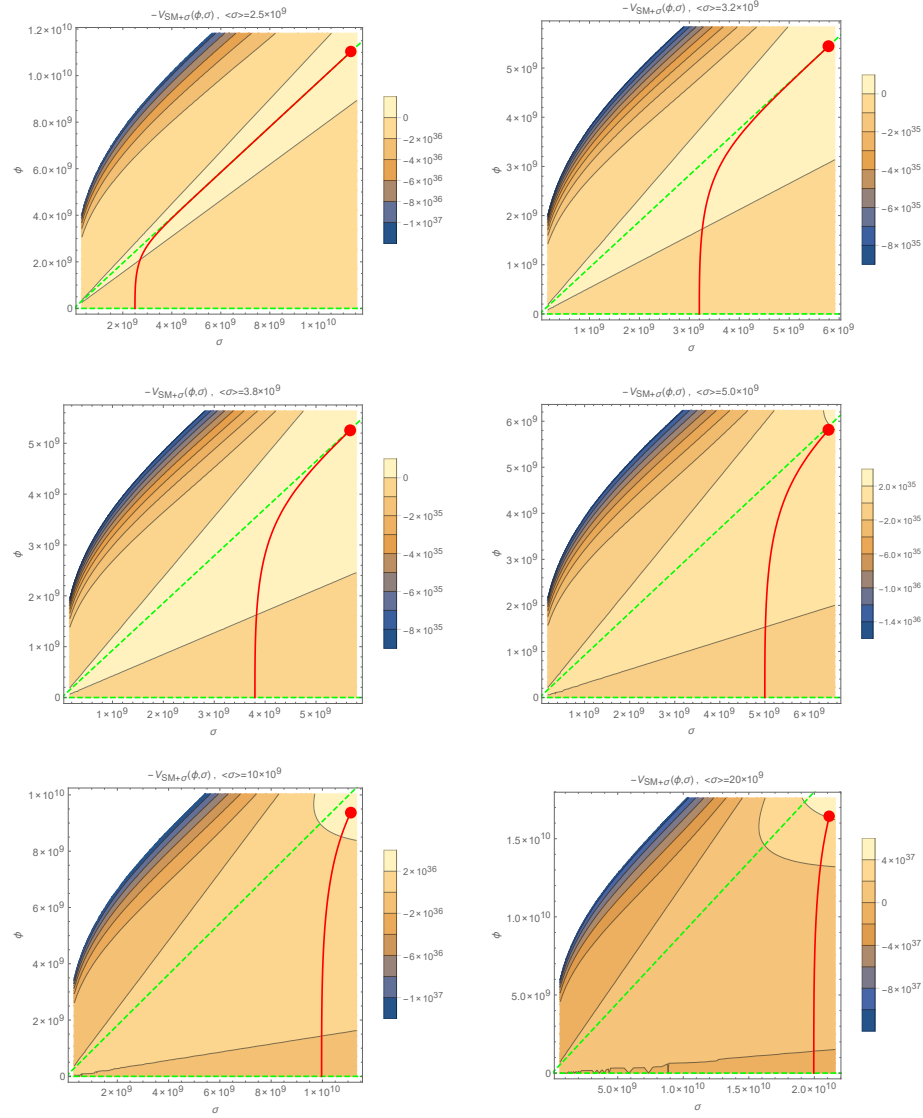


FIG. 2. Contour plots of the effective potentials $-V_{SM+\sigma}(\phi, \sigma)$ for various choices of $\langle \sigma \rangle$. Lower green dashed line marks the electroweak vacuum-direction, higher green dashed line marks the direction of greatest instability. Red continuous line is a plot of the bounce configuration (ϕ_B, σ_B) . (Note that, mainly due to varying contribution of the nonrenormalizable interaction from one plot to another, the plots present differing potentials and it would be misleading to plot the bounce configurations in a single frame.)

Summary

SM + dilaton

- 1) You may use **a field as the scale μ** in Dim-Reg to preserve scale symmetry at the quantum level.
- 2) The price to pay: infinitely many nonpolynomial ϕ/σ operators and corresponding couplings: **nonrenormalizability**.
- 3) Minimal subtraction scheme involves **evanescent interactions**.
- 4) Presence of a **flat direction** ← tuning.
- 5) **Naturalness: aligning** the flat direction perpendicular to Higgs
- 6) **Instability = unboundedness below**

Summary cd

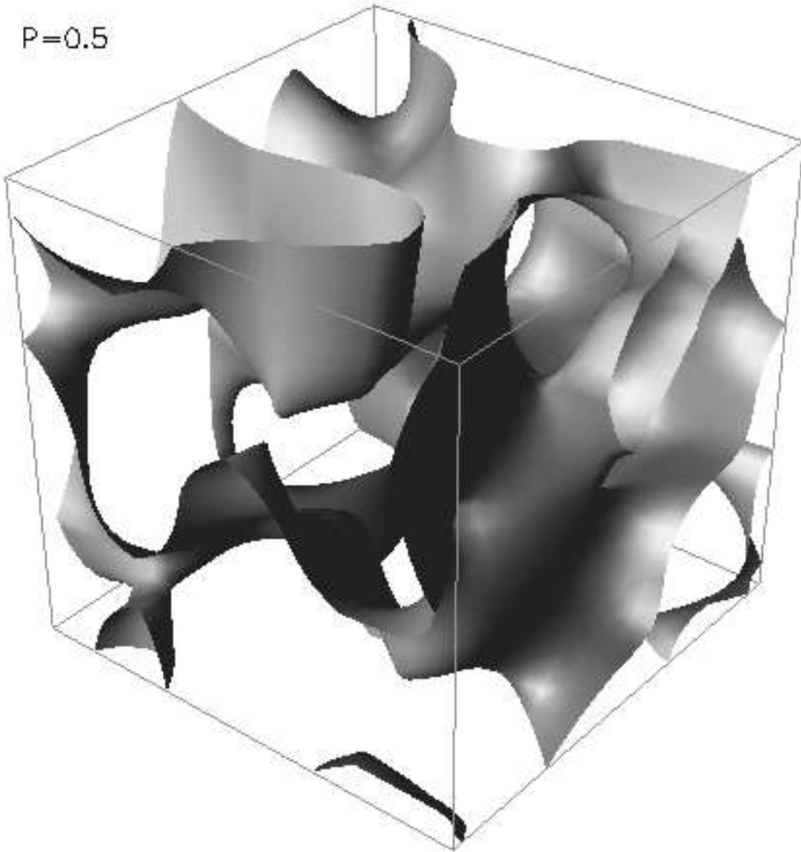
- Scale symmetry as the underlying symmetry offers a way to understand the origin of scales as expected
- Scale symmetry is broken at finite T with thermal dilaton vev proportional to T
- Cosmological evolution can easily lead to large dilaton vev needed to model hierarchy

Domain walls

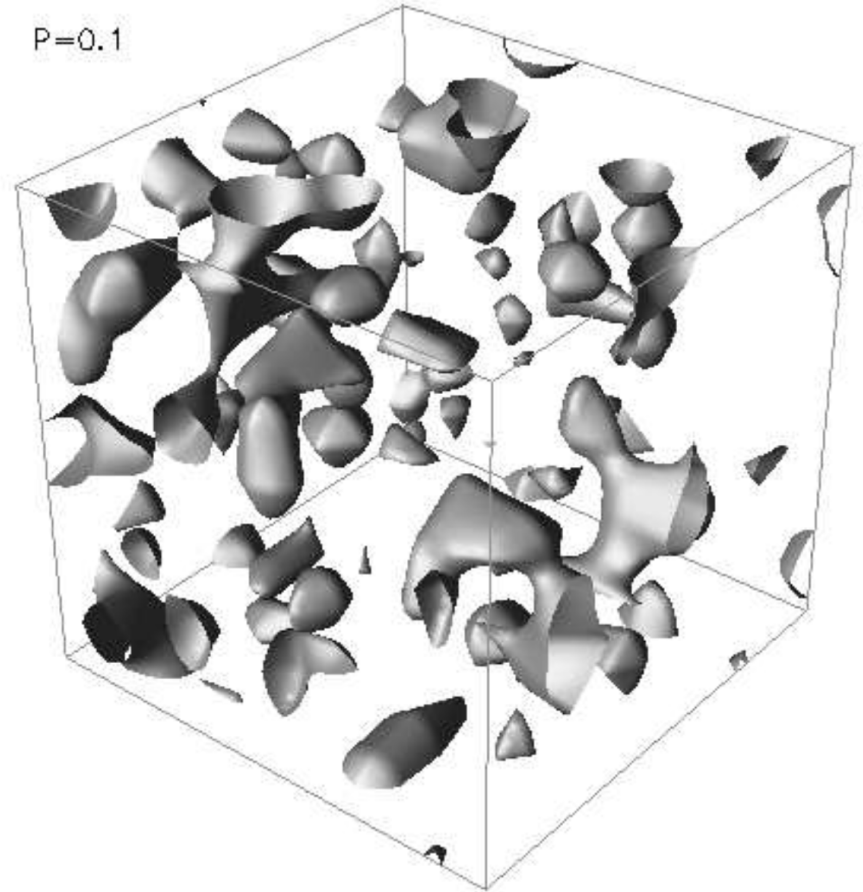
T. Krajewski, M. Lewicki
Phys. Rev. D **104**, 123522

Network of walls prefers the true vacuum!

$P=0.5$

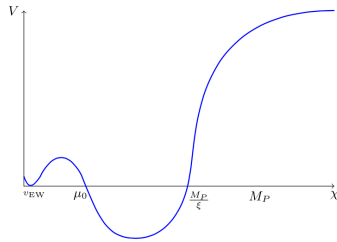


$P=0.1$

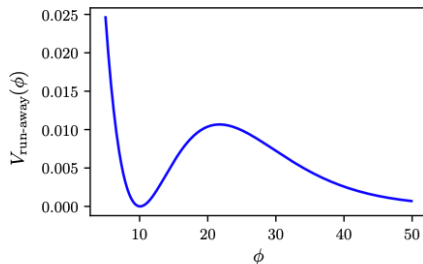


Models of interest

- Radiatively generated minima (eg SM at large field strength)



- Run-away potentials (moduli of stringy models), Quantum Scale Symmetric SM



- Models of strong first-order phase transitions - colliding bubbles (thermal effects play a role)

Generic potential

$$\begin{aligned}
 V_{AS}(\phi) = & \frac{V_0}{60} \phi (15\phi^3 (e^2 (2d(a+b+c) + ab + ac + bc + d^2) + 1) - 60abc (d^2 e^2 + 1) \\
 & - 20\phi^2 (e^2 (d^2(a+b+c) + 2d(a(b+c) + bc) + abc) + a + b + c) - 12e^2 \phi^4 (a + b + c + 2d) \\
 & + 30\phi (de^2(ad(b+c) + 2abc + bcd) + ab + ac + bc) + 10e^2 \phi^5). \quad (3.6)
 \end{aligned}$$

$$\begin{aligned}
 \frac{\partial^3 V_{AS}}{\partial \phi^3}(\phi) = & 2V_0 (e^2(a-\phi)(\phi-b)(c+2d-3\phi) \\
 & + (-a-b+2\phi) (e^2(d-\phi)(2c+d-3\phi) + 1) + (\phi-c) (e^2(d-\phi)^2 + 1)) \quad (3.7)
 \end{aligned}$$

a, b - positions of minima, c - position of maximum

$$\begin{aligned}
 \delta V &= V_{AS}(b) - V_{AS}(a), \\
 d^3 V &= \frac{\partial^3 V}{\partial \phi^3}(c), \\
 \delta &= w,
 \end{aligned}$$

Quantities of interest: energy density and peak frequency

$$\Omega_{GW}(\eta) := \frac{1}{\rho_c(\eta)} \frac{d\rho_{GW}}{d \log |k|}(\eta, k).$$

$$\Omega_{GW}(\eta_{dec})|_{peak} = \frac{\tilde{\epsilon}_{GW} \mathcal{A}^2 \sigma_{wall}^2}{24\pi H_{dec}^2 M_{Pl}^4},$$

$$\Omega_{GW}(\eta_0) = \left(\frac{a(\eta_{dec})}{a(\eta_0)} \right)^4 \left(\frac{H(\eta_{dec})}{H(\eta_0)} \right)^4 \Omega_{GW}(\eta_{dec})$$

Quantities of interest: energy density and peak frequency

$\tilde{\epsilon}_{GW}$ efficiency parameter between 0.7 and 1

$\sigma_{walls}, \eta_{dec}$ - taken from simulations

$$\frac{A}{V} = \frac{a(t)S_{wall}}{H^{-3}} \propto \frac{a(t)}{t}.$$

$$\frac{A}{V} = \mathcal{A}\eta^{-1},$$

stable DW: \mathcal{A} in the range 0.8 ± 0.1

Quantities of interest: energy density and peak frequency

more generally

$$\log \left(\frac{A}{V} \right) = -\nu \log \eta + \log \mathcal{A}$$

scaling regime: obtained ν ranges from 0.81 to 1.0

meta-stable DW: \mathcal{A} in the range 0.08 – 0.34

Scaling regime

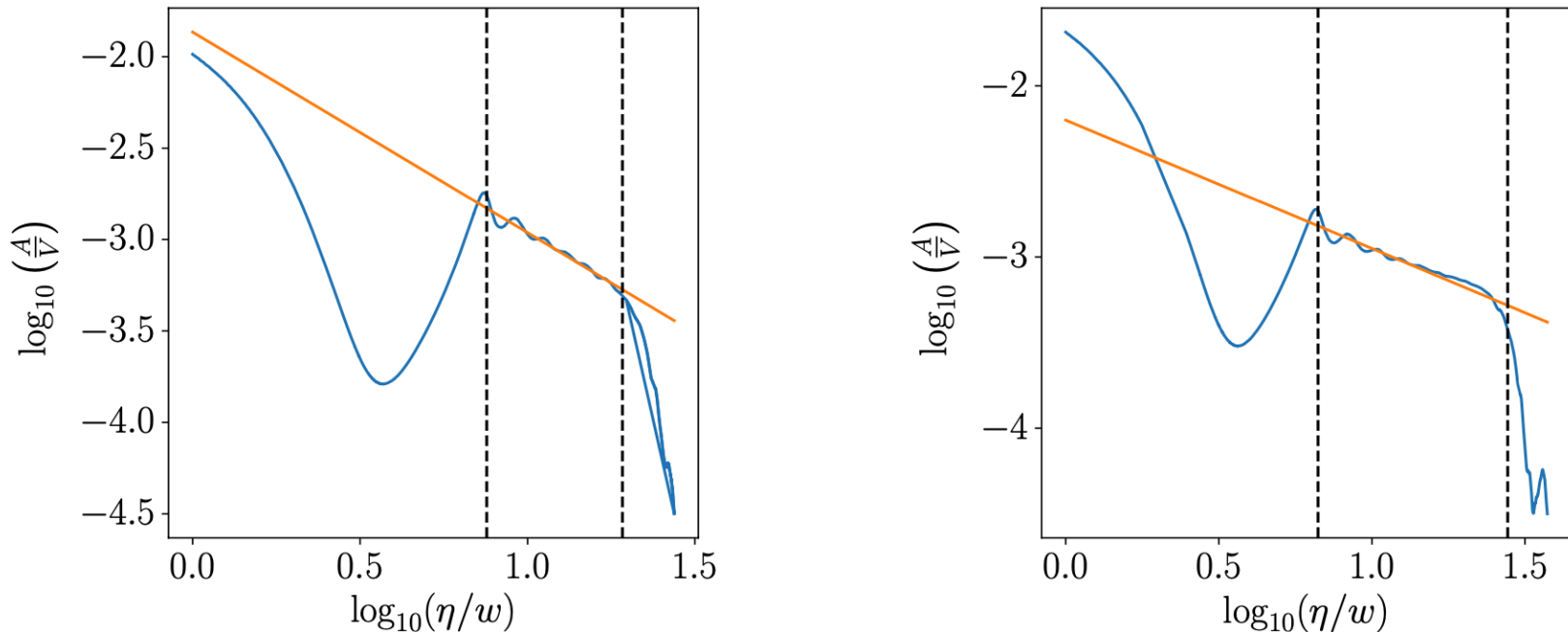


Figure 9: The evolution of conformal surface area of domain walls per unit volume $\frac{A}{V}$ in function of conformal time η (blue) and the fitted scaling behavior defined by eq. (5.8) (orange) for the best (left panel) and the worst (right panel) fits obtained by procedure described in the main text. Vertical dashed lines correspond to the estimated beginning and end of the scaling regime.

Quantities of interest: energy density and peak frequency

$$\Omega_{GW}(\eta_0)|_{peak} = 4.6 \times 10^{-81} \mathcal{A}^2 \left(\frac{\text{GeV}}{H_{dec}} \right)^2 \left(\frac{\sigma_{wall}}{\text{GeV}^3} \right)^2 h^{-2} \left(\frac{100}{g_*(\eta_{dec})} \right)^{\frac{1}{3}}.$$

$$f_0|_{peak} = \frac{a(\eta_{dec})}{a(\eta_0)} H_{dec} = 1.63 \times 10^2 \left(\frac{H_{dec}}{\text{GeV}} \right)^{\frac{1}{2}} \text{ Hz},$$

$$\Omega_{GW}(\eta_0)|_{peak} = 0.29 \times 10^{-77} \mathcal{A}^2 \left(\frac{\eta_{dec}}{w} \right)^4 \left(\frac{\sigma_{wall}}{w^{-3}} \right)^2 \left(\frac{\text{GeV}^{-1}}{w} \right)^4,$$

$$f_0|_{peak} = 3.3 \times 10^1 \left(\frac{w}{\eta_{dec}} \right) \left(\frac{\text{GeV}^{-1}}{w} \right)^{\frac{1}{2}} \text{ Hz},$$

Quantities of interest: energy density and peak frequency

We have estimated overall factors present in eqs. (6.7) and (6.7) basing on values of \mathcal{A} , η_{dec} obtained in simulations in which networks entered scaling regime and previously computed σ_{wall} . The maximal value of the prefactor in eq. (6.7) obtained in this way is equal to:

$$\Omega_{GW}^{max}(\eta_0)|_{peak} = 0.1 \times 10^{-66} \left(\frac{1 \frac{\hbar c}{\text{GeV}}}{w} \right)^4, \quad f_0^{max}|_{peak} = 0.7 \left(\frac{1 \frac{\hbar c}{\text{GeV}}}{w} \right)^{\frac{1}{2}} \text{ Hz}, \quad (6.9)$$

where the frequency of the peak for this network is denoted as f_0^{max} . On the other hand, the minimal prefactor computed from data from simulations is equal to:

$$\Omega_{GW}^{min}(\eta_0)|_{peak} = 0.6 \times 10^{-68} \left(\frac{1 \frac{\hbar c}{\text{GeV}}}{w} \right)^4, \quad f_0^{min}|_{peak} = 1.3 \left(\frac{1 \frac{\hbar c}{\text{GeV}}}{w} \right)^{\frac{1}{2}} \text{ Hz}. \quad (6.10)$$

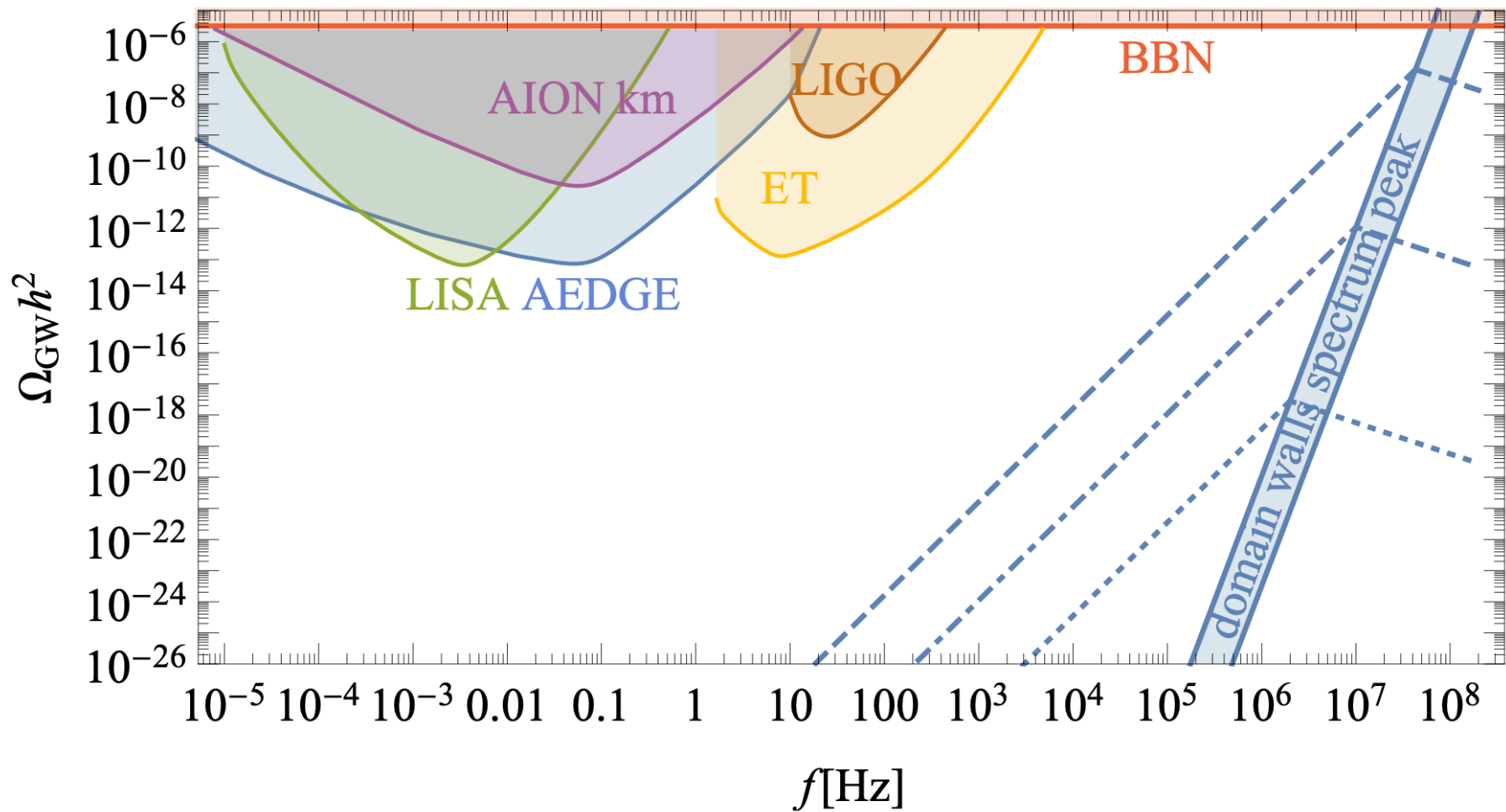


Figure 10: Hypothetical peak amplitudes of GWs emitted from cosmological domain walls as a function of the peak frequency f compared to predicted sensitivities of current and planned detectors LIGO [59–62], LISA [63, 64], AEDGE [65], AION-1km [66], ET [67, 68] as well as upper bound induced by the CMB/BBN [69, 70].

Partial Summary

- For a strong signal and a low frequency peak a period of stable evolution is needed
- Bias of the initial distribution easily destabilises the network
- Asymmetry of the potential destabilises the network for symmetric distributions
- Short living networks may give a strong signal if the energy scale is very large - but this produces a high frequency peak, beyond current sensitivity
- Decaying networks of domain walls produce a signal in the form of gravitational waves - too weak to be detected anytime soon - if a signal is detected then either fine-tuning or non-standard cosmology have occurred

Bumpy axion inflation

With Ogan Ozsoy
JCAP 01 (2021) 040

$$V(\phi) = \frac{1}{2}m^2\phi^2 + \Lambda^4 \frac{\phi}{f} \sin\left(\frac{\phi}{f}\right)$$

$$\Lambda^4 \lesssim m^2 f^2$$

“bumpy regime”

$$\frac{\mathcal{L}}{\sqrt{-g}} = \frac{M_{\text{pl}}^2}{2}R - \frac{1}{2}\partial_\mu\phi\partial^\mu\phi - V(\phi) - \frac{1}{4}F_{\mu\nu}F^{\mu\nu} - \frac{\alpha_c}{4f}\phi F_{\mu\nu}\tilde{F}^{\mu\nu}$$

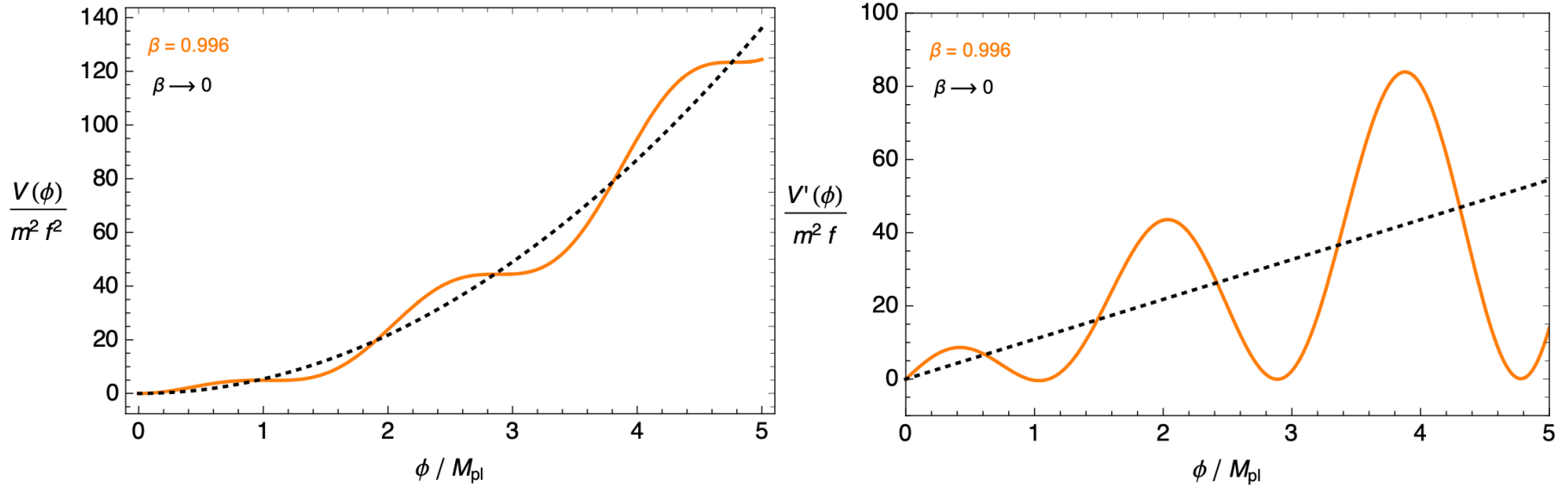


Figure 1: Potential $V(\phi)$ (left) in (1.1) and its derivative $V'(\phi)$ (right) for parameters $\beta \equiv \Lambda^4/m^2 f^2 = 0.996$ and $M_{\text{pl}}/f = 3.3$. For comparison we also plot the potential in the $\beta \rightarrow 0$ limit, *i.e.* for smooth quadratic potential $V(\phi) \propto \phi^2$ (black, dotted).

Note the vector modes

$$A''_{\pm}(x) + \left(1 \pm \frac{2\xi(x)}{x}\right) A_{\pm}(x) = 0, \quad (2.5)$$

where we defined dimensionless variable $-k\tau = x$. Realize that with our conventions ($\dot{\phi} < 0$ or $\xi > 0$), time dependent mass term in (2.5) can trigger tachyonic instability only for the negative helicity state A_- for modes satisfying $-k\tau < 2\xi$.

In the presence of gauge field production, the coupling $\phi F\tilde{F}$ may significantly affect inflaton fluctuations through the inverse decay of amplified fluctuations in the gauge field sector: $\delta A + \delta A \rightarrow \delta\phi$. In order to investigate these effects, we will focus on the mode equation of the canonical variable $\hat{Q}_\phi = a\delta\phi$, which can be derived from (3.4) as

$$\left(\partial_\tau^2 + k^2 + m_{\text{eff}}^2(\tau)\right) \hat{Q}_\phi(\tau, \vec{k}) = \hat{J}_\phi(\tau, \vec{k}) \equiv \frac{\alpha_c a^3}{f} \int \frac{d^3p}{(2\pi)^{3/2}} \hat{E}_i(\tau, \vec{k} - \vec{p}) \hat{B}_i(\tau, \vec{p}). \quad (3.8)$$

In terms of the slow-roll parameters and background quantities, the time dependent mass term is given by

$$m_{\text{eff}}^2(\tau) = -(aH)^2 \left[2 - \epsilon + \frac{3\eta}{2} + \frac{1}{4}\eta^2 - \frac{1}{2}\epsilon\eta + \frac{\dot{\eta}}{2H} \right], \quad (3.9)$$

where we defined

$$\epsilon \equiv \frac{\dot{\phi}^2}{2H^2 M_{\text{pl}}^2}, \quad \eta \equiv \frac{\dot{\epsilon}}{\epsilon H}. \quad (3.10)$$

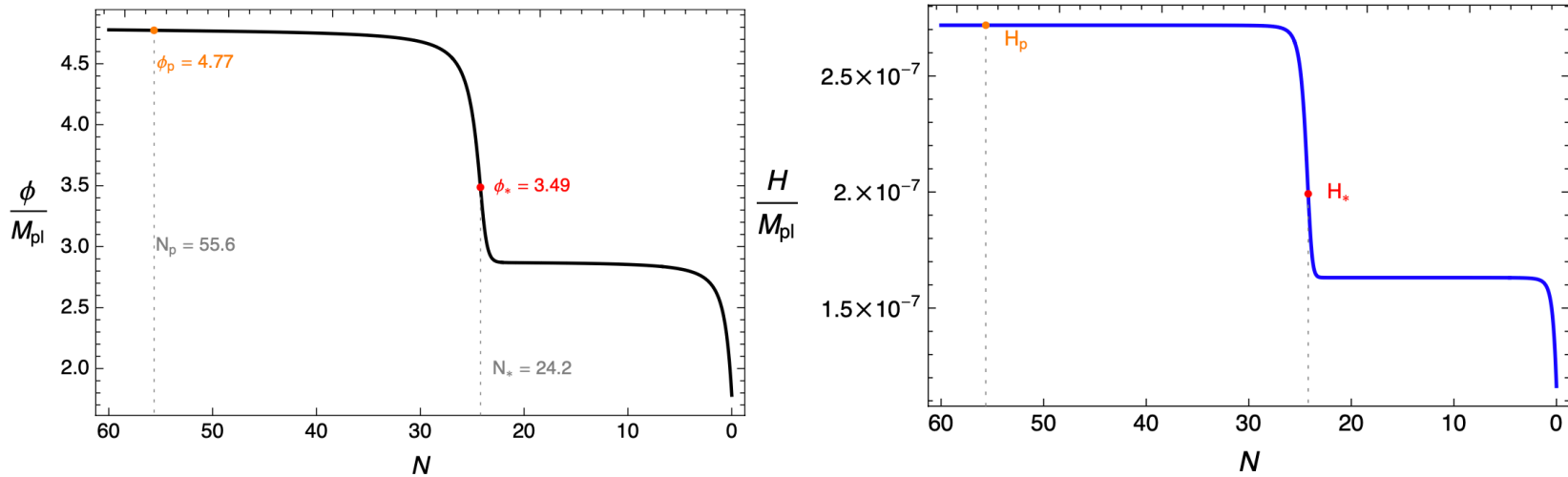


Figure 2: The evolution of ϕ (left) and Hubble parameter H (right) with respect to e-folds for the parameter choices given by (4.1) (See also Table 1) in the potential (1.1).

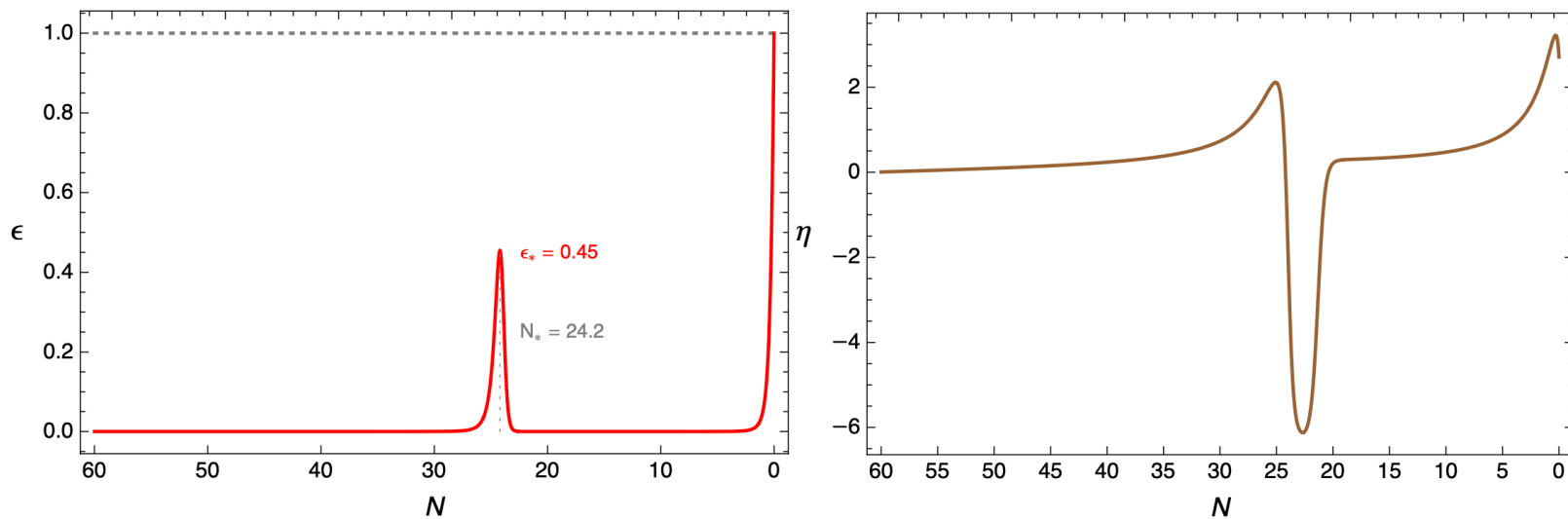


Figure 3: The evolution of slow-roll parameters ϵ (left) and η (right) with respect to e-folds during inflation for the same parameter choice provided in Figure 2.

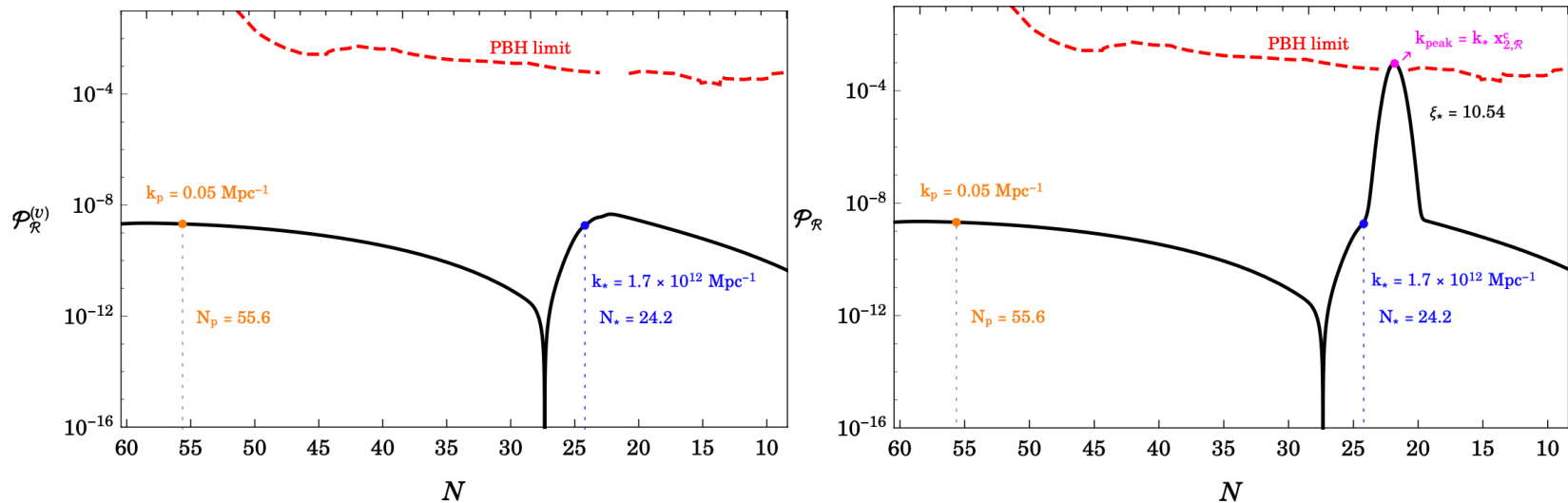


Figure 4: The vacuum power spectrum $\mathcal{P}_{\mathcal{R}}^{(v)}$ (left) and the total power spectrum in eq. (4.4) (right) as a function of number of e-folds in the bumpy axion monodromy model we studied in Section 4.1. On the right panel, the parameter choice $\xi_* = 10.54$ corresponds to *i.e.* $F_{\text{PBH}} = 1$ where PBHs constitutes the total DM abundance.

4.3.2 Primordial and Induced GW background from bumpy axion inflation

In the inflationary scenario we introduced above, there are two¹⁸ distinct populations of SGWB:

1. The GW background that originates from the amplified gauge fields during inflation through the channel: $\delta A_- + \delta A_- \rightarrow h_-$ which we study in Section 3.2. We label this contribution as “primordial”.
2. The induced GW background that originates from the scalar fluctuations that are enhanced by the gauge fields during inflation. The induced GW signal in this case is associated with the enhanced scalar modes that re-enter the horizon to form PBHs during RDU. We label this contribution as “induced” and study its production channel: $\delta A_- + \delta A_- + \delta A_- + \delta A_- \rightarrow \mathcal{R} + \mathcal{R} \rightarrow h_{\pm}$ in Appendix B.

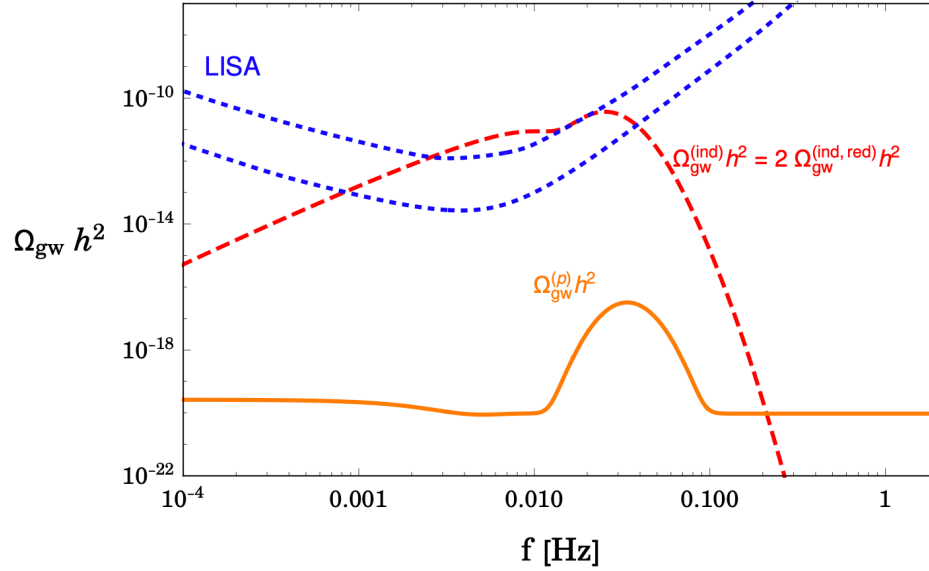


Figure 5: Primordial (orange solid) and induced (red dashed) contributions to the total SGWB presented in eq. (4.9) for the bumpy axion inflation. As explained in the main text, to estimate the total contribution to the induced signal, we multiplied the power spectrum of “Reducible” diagram $\mathcal{P}_\lambda^{(\text{ind,red})}$ by two (See *e.g.* eq. (C.12) of Appendix B).

Comments

- In Section 4.1 and 4.2 we have seen that the presence of pronounced modulations in the axion potential (See eq. (1.1) and Figure 1) alter inflationary dynamics in a way to provide sufficient amount of inflation even for an intermediate range of field excursions $\Delta\phi/M_{\text{pl}} \simeq \mathcal{O}(1)$ [80]. In particular, the existence of smooth plateaus in the potential leads to relatively small scale of inflation with a smaller tensor-to-scalar ratio $r \approx 10^{-5}$ at CMB scales when compared to models that exhibit smooth monomial terms in its scalar potential.
- In Section 4.3.1, we showed that in the presence of the coupling in eq. (1.2), the motion of ϕ around the cliff-like region of its potential triggers an instability for vector fields which in turn efficiently amplify the curvature power spectrum through $\delta A_+ + \delta A_- \rightarrow \mathcal{R}$, leading to a pronounced bump in the scalar power spectrum, see *e.g.* right panel of Figure 4. We have seen that these scalar fluctuations can later collapse into PBHs of mass $M \simeq 10^{-13} M_\odot$ which can constitute the total dark matter abundance in the universe.

Comments cd

In Section 4.3.2, we found that this large population of PBHs is accompanied by an unavoidable SGWB at LISA scales (See Figure 5) due to the non-linear nature of gravity [59–63]. As a primordial mechanism that leads to these findings at sub-CMB scales, the strongly non-Gaussian nature of scalar fluctuations (which obeys χ^2 statistics) in bumpy axion inflation can be considered as a distinguishing feature compared to single-field inflationary scenarios [160–162] and astrophysical backgrounds [163] which are expected to be Gaussian to a high degree. For example, compared to a Gaussian model of peaked scalar fluctuations at sub-CMB

Non-minimal curvaton - revisited

A, Ghoshal, C. Chen, Y. Luo, A. Naskar JCAP (2023)
D. Langlois, S. Pokorski, K. Turzyński JCAP 07 (2007) 014

$$S = \int d^4x \sqrt{-g} \left[\frac{M_{\text{Pl}}^2}{2} R - \frac{1}{2} \nabla_\mu \phi \nabla^\mu \phi - \frac{1}{2} \lambda^2(\phi) \nabla_\mu \chi \nabla^\mu \chi - V(\phi, \chi) \right]$$

$$V_{\text{cur}}(\chi) = f_a^2 m_\chi^2 \left(1 - \cos \frac{\chi}{f_a} \right)$$

Case study: the Gaussian-like dip

$$\lambda(\phi) = \lambda_c \left\{ 1 - A \exp \left[-\frac{(\phi - \phi_{\text{dip}})^2}{2\sigma_\lambda^2} \right] \right\}$$

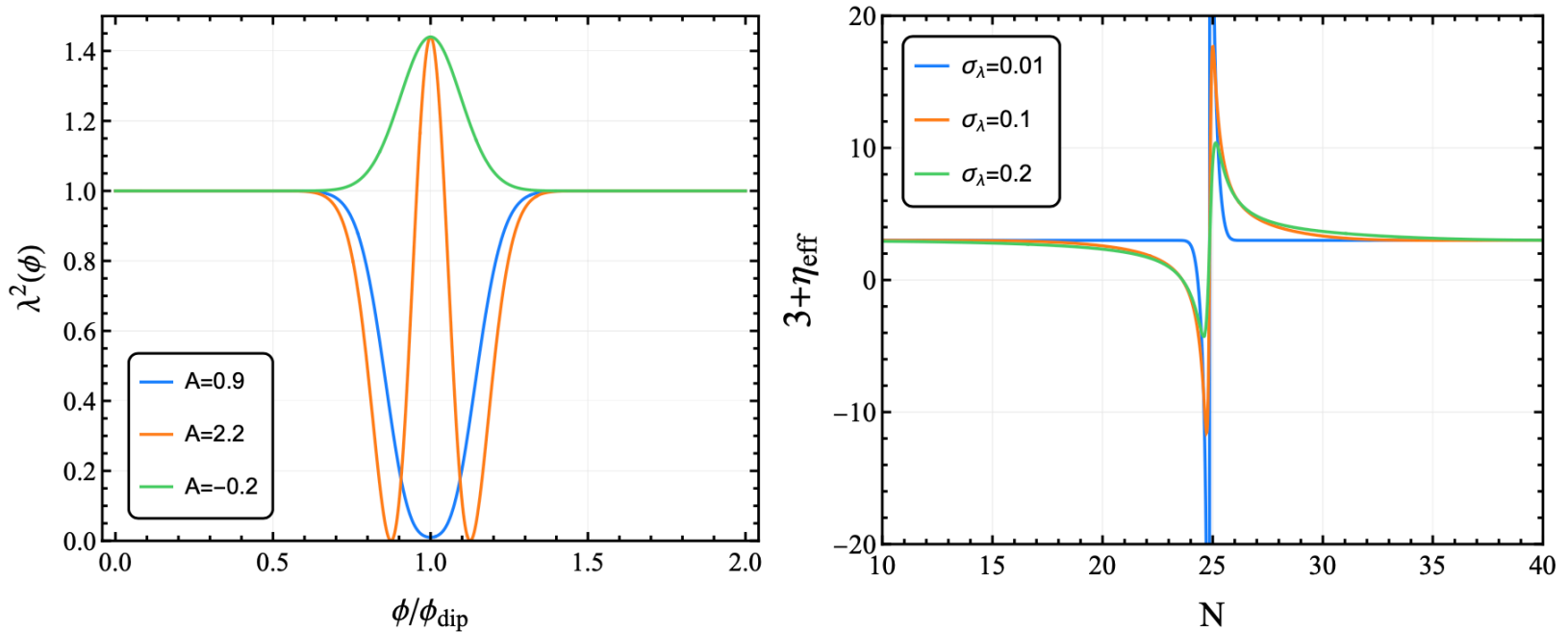


Figure 1. *Left panel:* An illustration of the field metric $\lambda^2(\phi)$ in terms of three typical values of A : 0.9 (blue), 2.2 (orange) and -0.2 (green), with the same width $\sigma_\lambda = 0.1$. This work only focuses on the first case $0 < A < 1$. *Right panel:* The numerical results of $3 + \eta_{\text{eff}}$ during the Starobinsky inflation for $\sigma_\lambda = (0.01, 0.1, 0.2)$ shown by the blue, orange and green curves, respectively. The parameters are taken as: $m_\chi/M_{\text{Pl}} = 10^{-8}$, $\phi_{\text{ini}}/M_{\text{Pl}} = 5.5$, $\phi_{\text{dip}}/M_{\text{Pl}} = 4.8$, $A = 0.995$, $\sigma_\lambda = 0.01$ and $\Lambda^4/M_{\text{Pl}}^4 \simeq 2 \times 10^{-14}$.

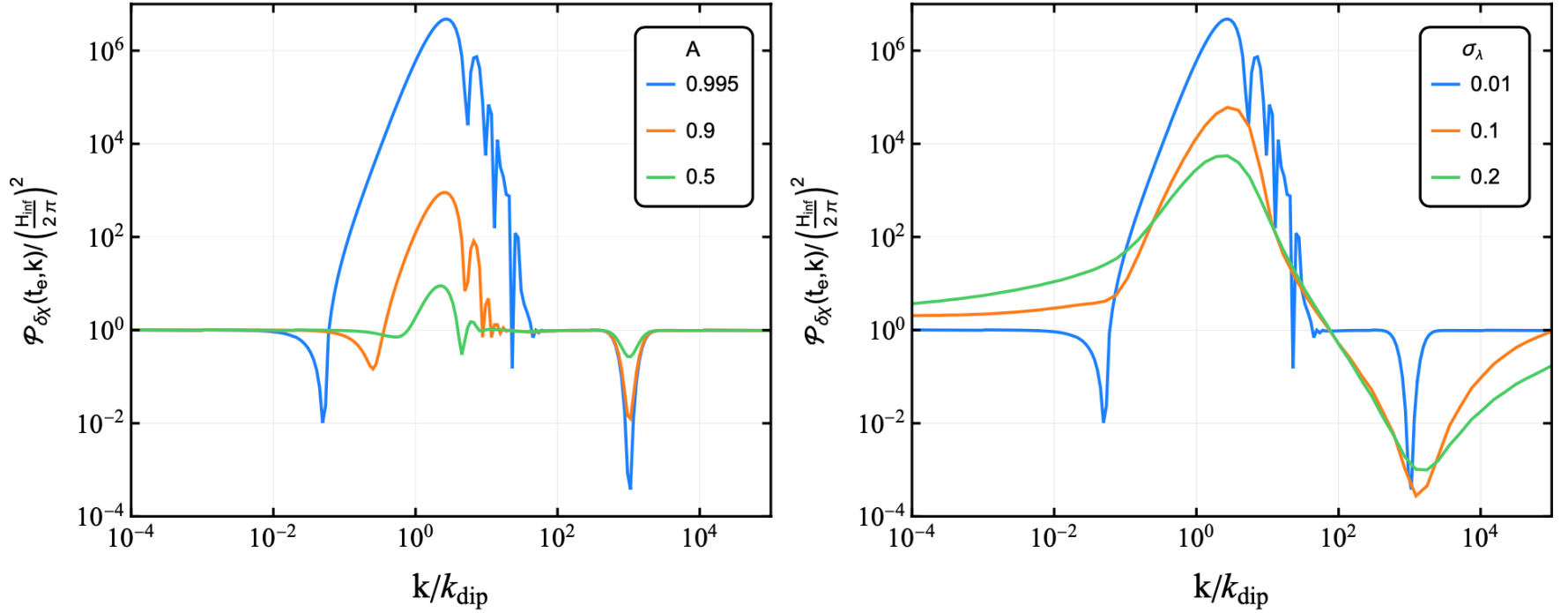


Figure 4. *Left panel:* The curvaton power spectra $\mathcal{P}_{\delta\chi}(t_e, k)$ in terms of various values $A = (0.995, 0.9, 0.5)$ for a fixed value $\sigma_\lambda = 0.01$. *Right panel:* The curvaton power spectra $\mathcal{P}_{\delta\chi}(t_e, k)$ in terms of various values $\sigma_\lambda = (0.01, 0.1, 0.2)$ for a fixed value $A = 0.995$. All other parameters are the same as Fig. 2.

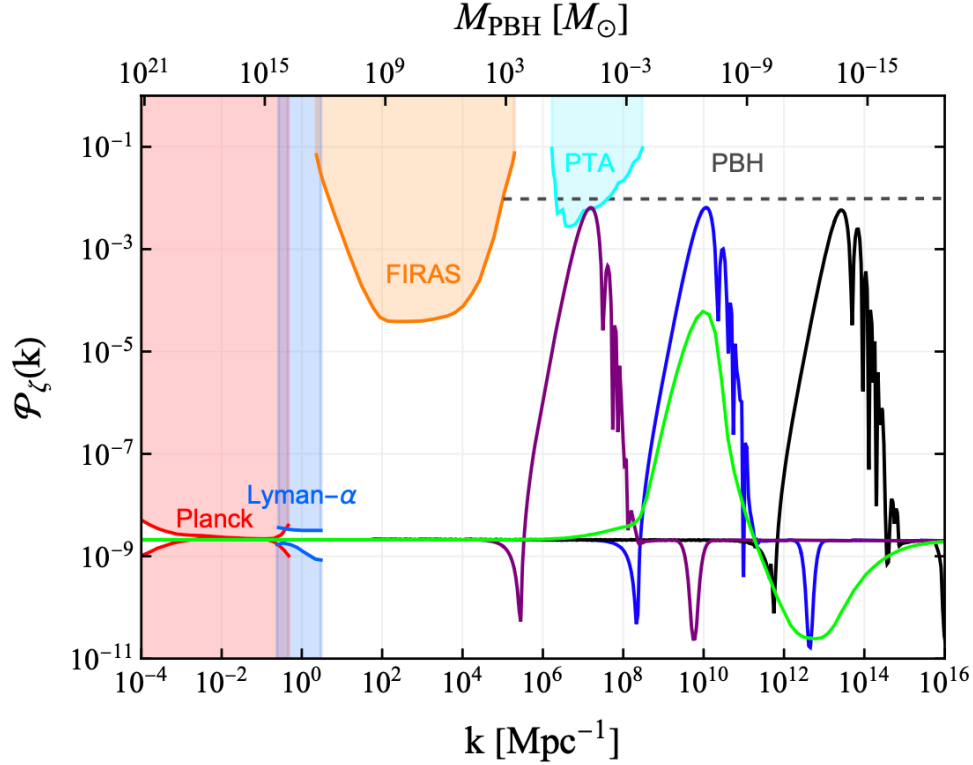


Figure 7. The numerical results of final curvature power spectrum $\mathcal{P}_\zeta(t_{\text{dec}}, k)$ at the curvaton's decay in terms of four set of parameters: $\{\phi_{\text{dip}}/M_{\text{Pl}} = 4.8, \sigma_\lambda = 0.01\}$ (the blue curve); $\{\phi_{\text{dip}}/M_{\text{Pl}} = 4.5, \sigma_\lambda = 0.01\}$ (the black curve); $\{\phi_{\text{dip}}/M_{\text{Pl}} = 5.0, \sigma_\lambda = 0.01\}$ (the purple curve); $\{\phi_{\text{dip}}/M_{\text{Pl}} = 4.8, \sigma_\lambda = 0.1\}$ (the green curve), and the rest parameters are the same with Fig. 2. The current constraints on $\mathcal{P}_\mathcal{R}(k)$ from Planck [1], Lyman- α [63], FIRAS [64] and PTA [24] are shown by the shadowed regions, while the grey dashed line refers to $\mathcal{P}_\mathcal{R} \sim 10^{-2}$ in order to produce an abundance of PBHs.

We plot $f_{\text{PBH}}(M)$ in Fig. 8 in terms of three spectra (blue, black and purple curves) shown in Fig. 7, and the power spectrum shown by the green curve only produce small fraction of PBHs that is not shown in Fig. 8. Note that the produced PBH fraction shown by the black curve is able to account for the whole dark matter.

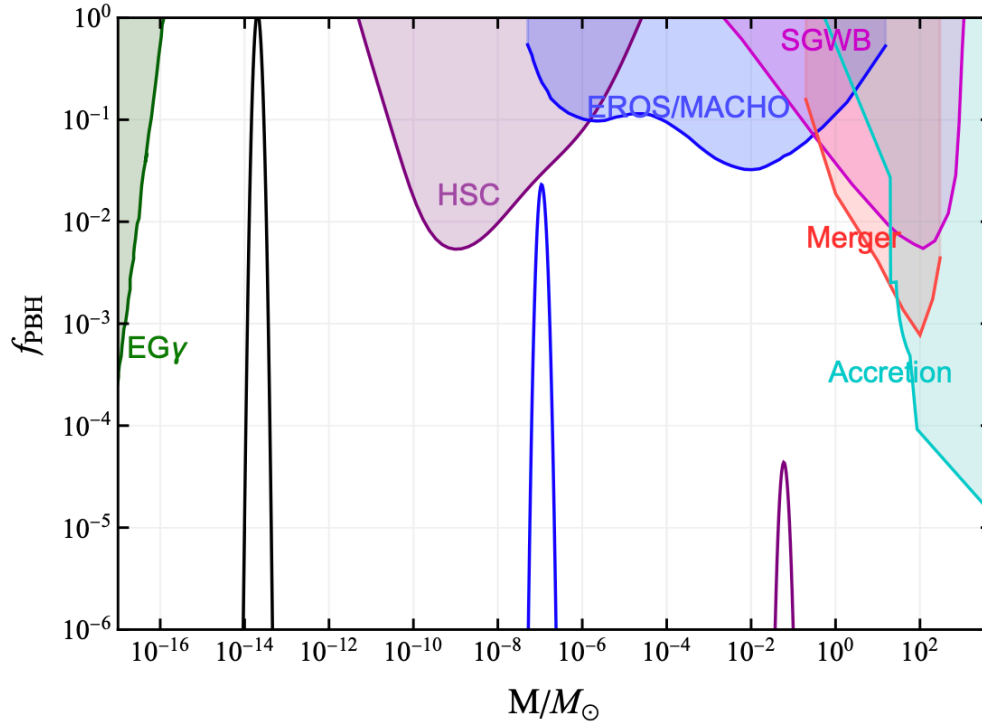


Figure 8. The current PBH abundance f_{PBH} in terms of three sets of parameters corresponding to the spectra (the black, blue and purple curves) shown in Fig. 7, with various constraints on f_{PBH} adopted from Ref. [6].

Scalar-induced gravitational waves

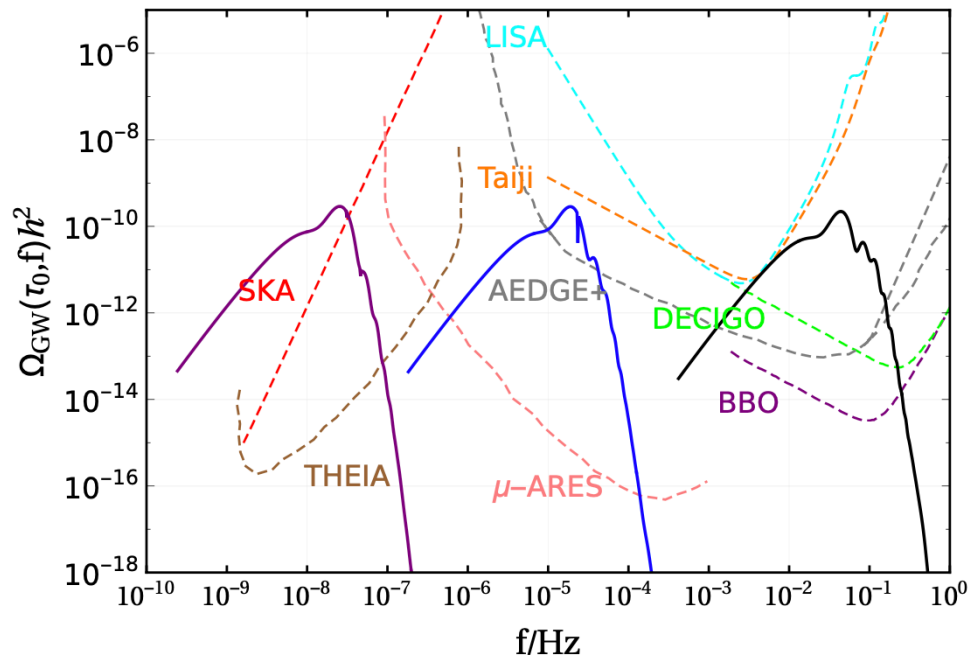


Figure 9. The current energy spectra $\Omega_{\text{GW}}(\tau_0, f)$ corresponding to three curvature spectra (the black, blue and purple curves) shown in Fig. 7, along with various GW experiments shown in Ref. [85].

The NANOGrav 15-year Data Set: Search for Signals from New Physics

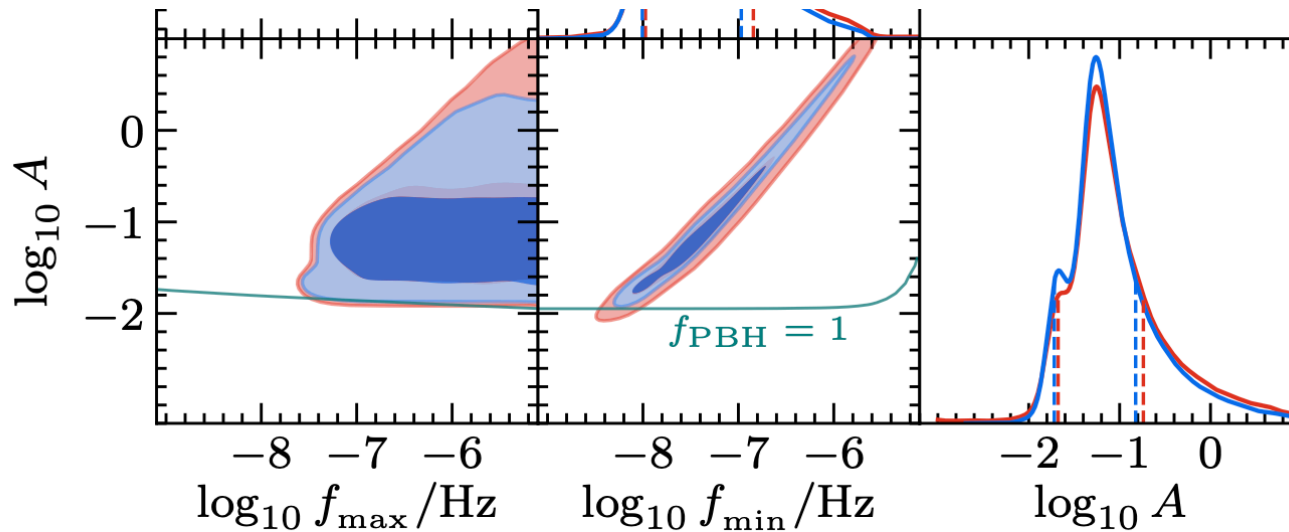


Figure 6. Same as in Fig. 5 but for the SIGW-BOX model. The regions *above* the teal contour lines labeled $f_{\text{PBH}} = 1$ lead to the overproduction of PBHs, according to our analysis in Appendix C.2; however, see text for more discussion.

Scalar-induced gravitational waves

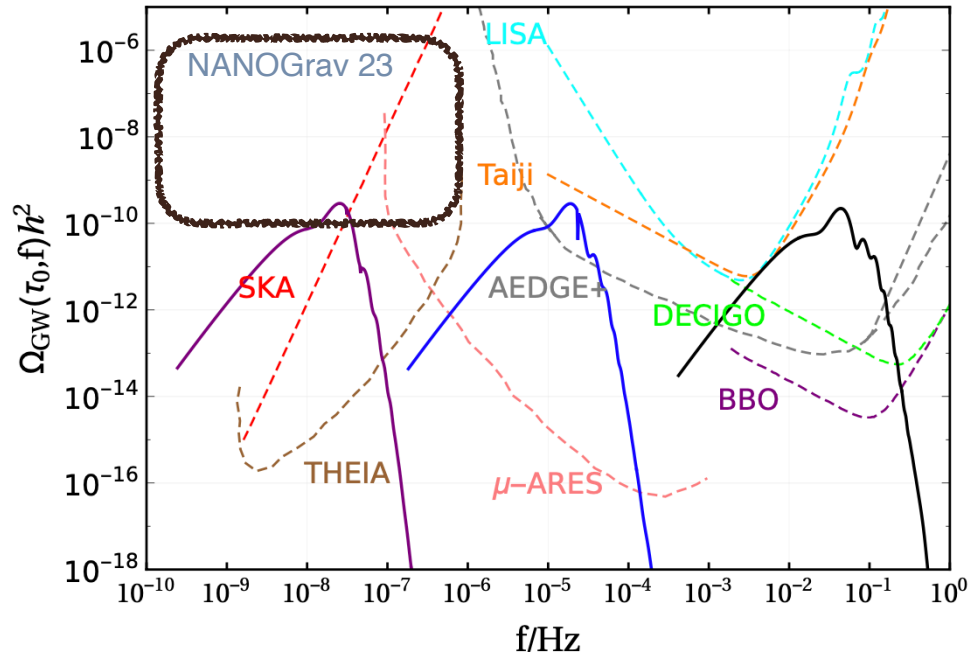


Figure 9. The current energy spectra $\Omega_{\text{GW}}(\tau_0, f)$ corresponding to three curvature spectra (the black, blue and purple curves) shown in Fig. 7, along with various GW experiments shown in Ref. [85].

Summary

- We have identified the role of the nontrivial metric in field space
- It plays a role of an effective friction term for curvaton perturbations
- Curvaton perturbations grow due to the presence of nontrivial kinetic coupling
- Case study - Gaussian-like dip in the field metric
- We have obtained analytically and numerically full spectrum of curvature fluctuations for axion-like curvaton potential
- Current PBH abundance in this model is sufficient to explain whole DM and concomitant SIGW signals are detectable

